ELSEVIER

Journal of Alloys and Compounds 270 (1998) 88–94

Journal of ALLOYS AND COMPOUNDS

Reduction of magnesium orthovanadate $Mg_3(VO_4)_2$

Xiandong Wang[a], Hong Zhang[b], Wharton Sinkler[b], Kenneth R. Poeppelmeier[a,*], Laurence D. Marks[b]

[a]*Department of Chemistry, Northwestern University, Evanston, IL 60208, USA*
[b]*Department of Materials Science and Engineering, Northwestern University, Evanston, IL 60208, USA*

Received 16 July 1997; received in revised form 15 August 1997

Abstract

Reduction of polycrystalline and crystalline magnesium orthovanadate $Mg_3V_2O_8$ by hydrogen was investigated in the temperature range of 560–920°C. A single crystal of orthorhombic $Mg_3V_2O_8$ with a cation-deficient-spinel structure (25% of the magnesium atoms on octahedral sites are vacant) was transformed into cubic $Mg_3V_2O_6$ which has a cation-stuffed-spinel structure (8*a* and 16*c* sites were partially occupied by magnesium and 16*d* sites were fully occupied by magnesium and vanadium) at 560°C in 7% H_2 in N_2. © 1998 Elsevier Science S.A.

Keywords: $Mg_3V_2O_8$; $Mg_3V_2O_6$; Deficient-spinel; Stuffed-spinel

1. Introduction

Oxidative dehydrogenation of light alkanes by oxide catalysts is of great significance in the petrochemical industry. Multicomponent vanadates/molybdates that contain discrete VO_4/MoO_4 structural features often exhibit excellent catalytic properties in terms of high selectivity and conversion [1–5]. In the Mg–V–O system, magnesium orthovanadate $Mg_3V_2O_8$ has been shown to be an active phase for the oxidative dehydrogenation of butane to butenes and butadiene [3] and propane to propene [6]. The structure [7] is an orthorhombic magnesium deficient spinel-type structure $V_2^T(Mg_3\square)^OO_8$ (T: tetrahedral site, O: octahedral site, □: cation vacancy). Three distinct oxygen atoms (instead of one unique oxygen in normal spinel) form the nearly close packed oxygen layers, between which the octahedral magnesium and tetrahedral vanadium cations are located. The initial abstraction of hydrogen from alkanes, which is generally regarded as the rate-determining step [8], reduces the metal-oxide which is then reoxidized from gas phase or subsurface oxygen. Therefore, $Mg_3V_2O_8$ is a good model to understand how one of several components of an alkane dehydrogenation catalyst responds to reduction.

2. Experimental

Polycrystalline $Mg_3V_2O_8$ was prepared by solid state reaction from MgO and V_2O_5 at 900°C. The weight loss of $Mg_3V_2O_8$ was determined by Thermal Gravimetric Analysis (TGA) in a flowing gas of 7% H_2 in N_2. Polycrystalline $Mg_3V_2O_6$ was prepared by heating $Mg_3V_2O_8$ powder to 920°C for 12 h in flowing 7% H_2 in N_2. $Mg_3V_2O_8$ crystals were grown by flux methods: (i) Mixture of MgO and V_2O_5 (5:2 molar ratio) was heated to 1220°C (T_{max}), cooled to 1100°C at 2°C h^{-1}, and further cooled to room temperature at 60°C h^{-1}. Colorless or slightly yellow crystals with sizes ≤2 mm were readily obtained. (ii) Mixture of $MgMoO_4$ and $Mg_3V_2O_8$ (1:4 molar ratio) was heated to 1200°C, cooled to 1100°C at 6°C h^{-1}, and further cooled to room temperature at 60°C h^{-1}. Colorless plate crystals were obtained. $Mg_3V_2O_6$ crystals were obtained by reducing $Mg_3V_2O_8$ crystals in 7% H_2 in N_2. About 67 mg of $Mg_3V_2O_8$ crystals was first heated to 500°C at 2°C min^{-1} then to 560°C at 1°C min^{-1}, holding at 560°C for 60 h.

A black crystal with approximate dimensions of 0.17×0.13×0.11 mm was mounted on an Enraf-Nonius CAD4 diffractometer. Data were collected at −120°C with monochromated MoKα radiation and ω scans (some additional details of the data collection and refinement are listed in Table 1). The programs used for structure solution and

*Corresponding author. Fax: 001 847 4917713.

PII: S0925-8388(97)00471-4

Table 1
Crystal data for $Mg_3V_2O_6$ [a]

Chemical formula	$Mg_2V_{1.333}O_4$
Formula weight	180.36
Space group, Z	Fd-3m (No. 227), 8
a	8.409(2) Å
V	594.6(3) Å^3
D_x	4.03 g cm^{-3}
μ(Mo Kα)	45.5 cm^{-1}
$2\theta_{max}$	53.9°
No. of reflections measured	Total: 789
No. of observations ($I>3.00\sigma(I)$)	144
No. of variables	7
$R=\Sigma \|\|F_{obs}\|-\|F_{calc}\|\|/\Sigma \|F_{obs}\|$	0.028
$R_w^b=[\Sigma w(\|F_{obs}\|-\|F_{calc}\|)^2/\Sigma w\|F_{obs}\|^2]^{1/2}$	0.034
Goodness of fit	1.63
Final difference Fourier peaks (max, min)	0.55, −0.54 e$^-$/Å^3

[a]Further details of the crystal structure determination can be ordered from Fachinformationszentrum Karlsruhe, D-76344 Eggenstein–Leopoldshafen (Germany), on quoting the depository number CSD-406566.
[b]$w=1/\sigma^2(F_{obs})$.

refinement are the same as in [9]. An empirical absorption correction using the program DIFABS [10] was applied which resulted in transmission factors ranging from 0.73 to 1.00.

TPR was performed in a quartz reactor and flow gas of 5% H_2 in Ar (25 ml min^{-1}). After heating (8°C min^{-1}) to 800°C, the temperature was held at 800°C until the reaction approached completion. The amount of consumed hydrogen was calculated based on a standard curve which was calibrated by Cu_2O/SiO_2 powder. HRTEM imaging and electron diffractions were carried out using a Hitachi 9000 microscope operated at 300 kV. Infrared spectra were recorded on a Bio-Rad Fourier transform infrared spectrophotometer in the range 1500–400 cm^{-1}. Samples were prepared by mixing with KBr. Magnetic susceptibilities of $Mg_3V_2O_6$ were determined on a SQUID susceptometer (Quantum Design Corp., MPMS) between 5 and 300 K. About 54 mg $Mg_3V_2O_6$ powder and 11 mg $Mg_3V_2O_6$ crystals were encased in sealed gelatin capsules and zero field cooled to 5 K. A 1 kG field was used for all measurements.

3. Results and discussion

During reduction of $Mg_3V_2O_8$ one weight loss step of 10.4 wt.%, which corresponds to $Mg_3V_2O_6$, was observed with varying heating rates with complete reduction occurring by 560°C. The X-ray diffraction (XRD) pattern of $Mg_3V_2O_6$ was indexed with a cubic unit cell, a=8.4209(2) Å (Fig. 1A). Polycrystalline $Mg_3V_2O_6$ can be readily reoxidized to $Mg_3V_2O_8$ in air or oxygen at 500°C. This reversible phenomenon encouraged us to reduce $Mg_3V_2O_8$ single crystals grown from an off-stoichiometry flux composition determined by the phase diagrams of MgO–V_2O_5 [11] and $MgMoO_4$–$Mg_3V_2O_8$ [9]. After reduction in H_2, again a weight loss of 10.4 wt.% was observed, the crystals (Fig. 2) undergo a color change from colorless to black and maintain their shape. Consistent with Thermogravimetric Analysis (TGA) results, Temperature Programmed Reduction (TPR) (Fig. 3) revealed that one mole of polycrystalline or single crystal $Mg_3V_2O_8$ consumed two moles H_2. The relatively broad profile for the crystals

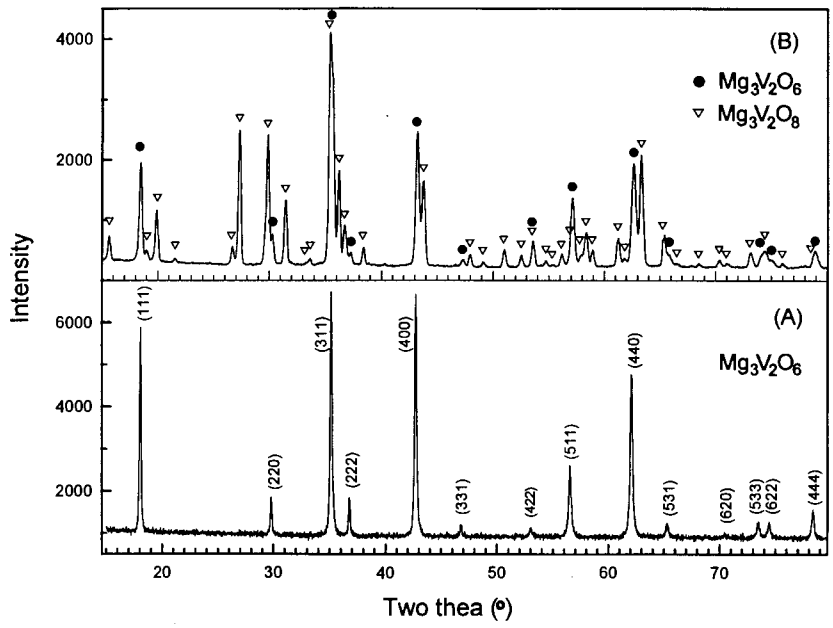

Fig. 1. XRD patterns of reduced $Mg_3V_2O_8$ samples in flowing 7% H_2 in N_2. (A) Reduction at 920°C for 12 h. Pure $Mg_3V_2O_6$ phase was obtained. A CuKα1 X-ray diffractometer with a LiF monochromator was used for data collection (step scan: 0.02°/50 s). (B) Reduction at 620°C for 1 h. A mixture with nominal composition $Mg_3V_2O_{7.47}$ was produced. A CuKα Rigaku X-ray diffractometer was used for data collection (step scan: 0.02°/10 s).

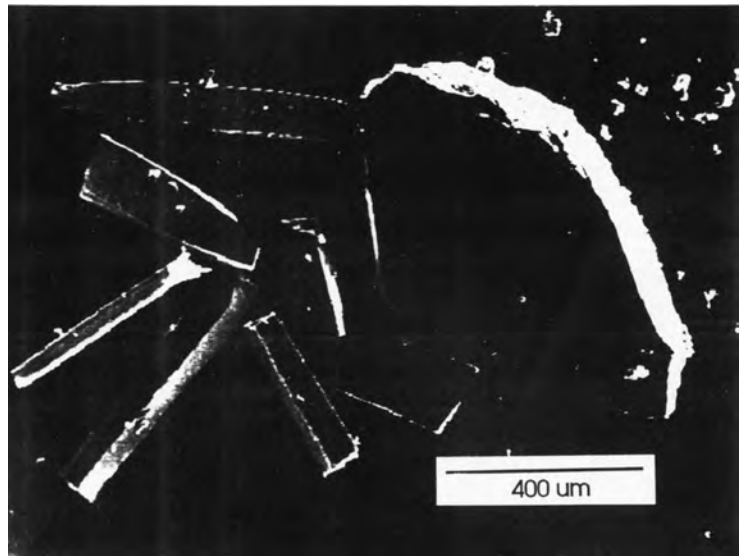

Fig. 2. SEM photograph of $Mg_3V_2O_6$ crystals.

reflects the small surface to volume ratio compared to the polycrystalline sample. Presumably the synthesis of $Mg_3V_2O_6$ is successful because of the relatively low reaction temperature and use of hydrogen as a reducing agent. $Mg_3V_2O_6$ was not reported in the high temperature study of the binary system $MgO–V_2O_3$ [12].

Single Crystal X-ray Diffraction Analysis determined that $Mg_3V_2O_6$ (or $Mg_2V_{1.333}O_4$) is a spinel structure with an excess of cations (Table 1). Energy Dispersive Analysis of X-ray (EDAX) on different areas of the investigated crystal gave the same atomic ratio of Mg:V=3:2 within the analytical errors. The vanadium atoms and 1/3 of the magnesium atoms occupy the 16*d* position, the remaining magnesium atoms are approximately equally distributed on the 8*a* and 16*c* positions. Partial cation occupancy on both the 8*a* and 16*c* sites is likely due to the strong coulombic repulsion created by the short distance (1.82 Å) between the two sites (Table 2). Similar cation distributions occur in $Li_2Mn_2O_4$ [13] (Occ (8*a*)=43%, Occ)=79%) and $Ni_{2.62}Ti_{0.69}O_4$ [14] (Occ (8*a*)=66%, Occ (16*c*)=28%). In

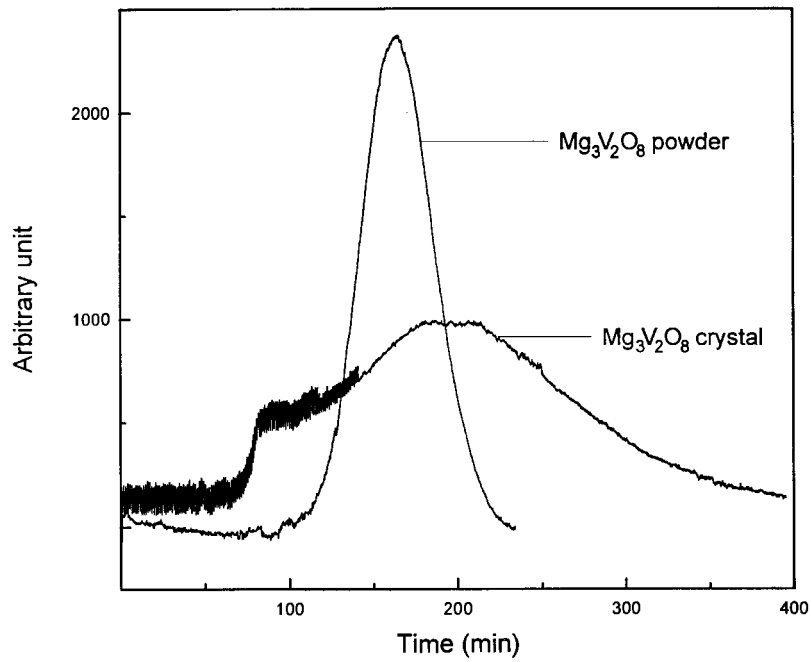

Fig. 3. TPR spectra of $Mg_3V_2O_8$ powder and crystals conducted in H_2/Ar at 800°C. 4.80×10^{-4} mol powder consumes 9.37×10^{-4} mol H_2 and 5.79×10^{-4} mol crystals consumes 1.08×10^{-3} mol H_2.

Table 2
Atomic coordinates, occupancy, isotropic displacement parameters and selected interatomic distances (Å) for $Mg_3V_2O_6$

Atom	Position	*x*	*y*	*z*	Occ	U_{iso} (Å^2)
Mg(1)	8*a*	0.125	0.125	0.125	2/3	0.0028(9)
Mg(2)	16*d*	0.5	0.5	0.5	1/3	0.0065(5)
V	16*d*	0.5	0.5	0.5	2/3	0.0065(5)
Mg(3)	16*c*	0	0	0	1/3	0.039(2)
O	32*e*	0.2574(2)	0.2574(2)	0.2574(2)	1.0	0.0110(6)
Distances						
Mg(1)–O	1.928(3)	Mg(1)–Mg(2)	3.4862(7)			
Mg(2)–O	2.042(2)	Mg(1)–Mg(3)	1.8206(1)			
Mg(3)–O	2.166(2)	Mg(2)–Mg(3)	2.9730(4)			

contrast are $Li_2Ti_2O_4$ [15] and $Li_2V_2O_4$ [16], in which all extra cations in the spinel-type structure reside on the 16*c* sites and the 8*a* sites are vacant. The distances between 16*c* and 16*d* and 8*a* and 16*d* are, respectively, 2.97 Å and 3.49 Å (Table 2), significantly longer distances than that between the 8*a* and 16*c* sites.

The reductive formation of $Mg_3V_2O_6$ from $Mg_3V_2O_8$ should be regarded as a change from a cation-deficient orthorhombic spinel to a cation-stuffed cubic spinel. A comparison of the two structures (Fig. 4) along the [**100**] direction for $Mg_3V_2O_8$ and the [**011**] direction for $Mg_3V_2O_6$ illustrates the close packed oxygen planes and the octahedral and tetrahedral interstices. In $Mg_3V_2O_8$ both O(1) and O(3) are three coordinate, each oxygen bonds to two magnesium atoms and one vanadium atom, while O(2) is four coordinate. The basic and coordinately-unsaturated O(1) and O(3) sites form cation deficient tunnels (Fig. 4A), which are possible pathways for the H_2 molecules to initiate reduction followed by dehydroxylation. Also it would not be surprising if the relative positions of Mg(1) and O(2) atoms in the Mg–O layers parallel to the *c* direction (Fig. 4A) remain essentially unchanged. Although the real reduction mechanism is unknown, the overall reaction model is:

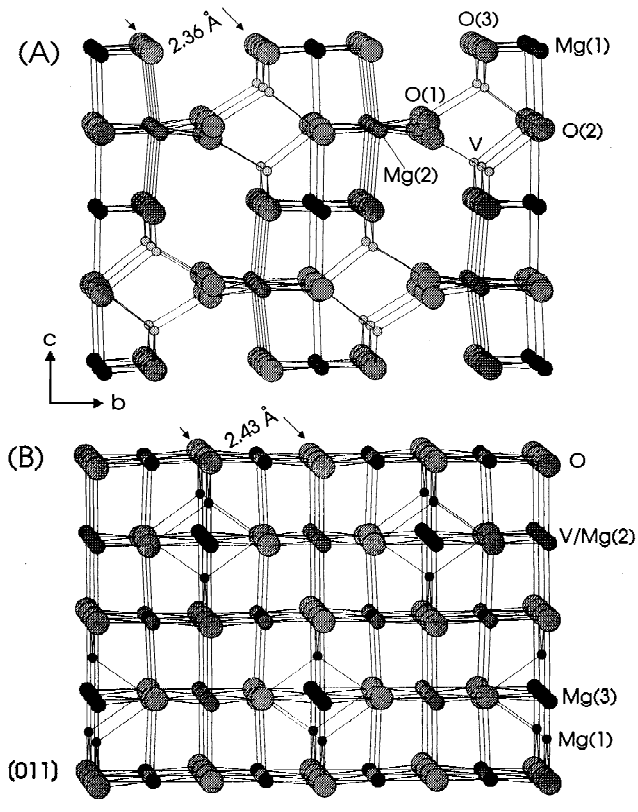

Fig. 4. Comparison of $Mg_3V_2O_8$ and $Mg_3V_2O_6$ structures. (A) $Mg_3V_2O_8$ ($a=6.053$ Å, $b=11.442$ Å, $c=8.330$ Å, S.G. *Cmca*, after [7]) viewed along the [**100**] direction. (B) $Mg_3V_2O_6$ viewed along the [**011**] direction. The close packed oxygen layers are marked by arrows and the distances between the layers are shown.

$$Mg_3V_2O_8: [V]^{t}_{32}[Mg(1)]^{o}_{16}[Mg(2)]^{o}_{32}[\square]^{o}_{16}O_{128} \rightarrow$$
$$\{[V]_{32}[Mg(2)]_{16}\}^{16d}[Mg(1)]^{8d}_{16}[Mg(3)]^{16c}_{16}O_{96}: Mg_3V_2O_6$$

The symbols t, o and square represent tetrahedral site, octahedral site and cation vacancy, respectively. In summary the vanadium atoms move to octahedral interstices and are disordered with Mg(1) (Fig. 4A), both of which are eventually on the 16*d* sites (Fig. 4B). The Mg(2) atoms (Fig. 4A) split into two groups and occupy the tetrahedral 8a and octahedral 16*c* sites equally (Fig. 4B).

Powder X-ray diffraction refinement by the FullProf Program [17] for polycrystalline $Mg_3V_2O_6$ is in good agreement with the model in Table 2. Other models, such as that with the extra cations on the 16*c* sites and vacancies on the 8*a* sites, or a model with fully occupied 8*a* and 16*d* sites and the extra cations on 16*c* sites, can not be refined reasonably.

High-Resolution Transmission Electron Microscopy (HRTEM) is a powerful technique to study the local structures of solid catalysts [18]. HRTEM results revealed unambiguously that $Mg_3V_2O_6$ is single phase. The XRD pattern of $Mg_3V_2O_6$ is very similar to that of a 2:1 molar mixture of MgO and MgV_2O_4 because the cell parameter of MgO ($a=4.213$ Å) is half that of the spinel MgV_2O_4 ($a=8.420$ Å). However, MgO was never observed by electron diffraction, imaging or EDAX in the polycrystalline $Mg_3V_2O_6$ powder samples. A cubic phase with lattice constant of about 8.2 Å, space group *Fd*-3*m*, was the

unique phase in all samples. Single crystals showed the same image as the polycrystalline material produced in the powder synthesis. For example, the [**112**] image is shown in Fig. 5. However, some areas in a few crystals revealed a mixture of $Mg_{3-x}V_2O_{6-x}$ and MgO, as marked in the [**001**] image in Fig. 6. The fine lattice fringes are MgO which was confirmed by fourier transform of the image. Image simulations based on the refined structural model in Table 2 also match very well with the experimental images (see Fig. 5).

Partially reduced samples always produced a mixture of white $Mg_3V_2O_8$ and black $Mg_3V_2O_6$ (Fig. 1B, Table 3) particles. The cell parameters of $Mg_3V_2O_8$ phase decrease very slightly when reduction takes place (Table 3). The a lattice constant of the $Mg_3V_2O_6$-type phase also decreases in the partially reduced samples compared to pure $Mg_3V_2O_6$ phase. The smaller *a* axis may be due to fewer excess cations in the structure and similar to that reported in cation-excess magnetite $Fe_{3+\delta}O_4$ [19]. Infrared (IR) studies (Fig. 7) revealed that the absorptions for $Mg_3V_2O_8$ in the range of 830–920 cm^{-1}, which are due to the vibration modes of VO_4 tetrahedra [20], diminish in the partially reduced samples and disappear in $Mg_3V_2O_6$ and two absorptions (619 and 462 cm^{-1}) appear, which are similar to those (625 and 485 cm^{-1}) found in MgV_2O_4 [20]. The IR spectra indicate that all the VO_4 tetrahedra in $Mg_3V_2O_8$ are converted to VO_6 octahedra in $Mg_3V_2O_6$ after reduction. Combining the XRD and IR studies, it appears that the reduction of V^{5+} in $Mg_3V_2O_8$ to V^{3+} in $Mg_3V_2O_6$ occurs without an intermediate V^{4+} state.

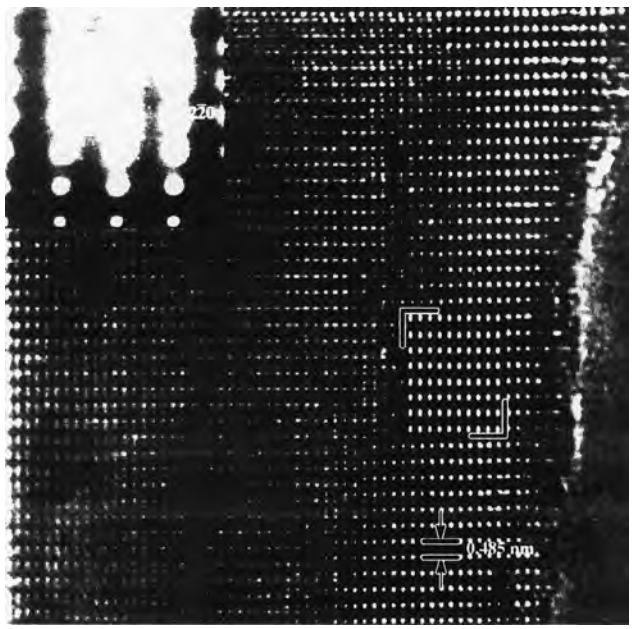

Fig. 5. HRTEM image of $Mg_3V_2O_6$ crystal along the [**112**] direction showing a homogenous pattern. Selected-Area Electron Diffraction (SAED) pattern and simulated image are shown in the insets. A good match to the experimental image is found for a thickness of 35 Å and a defocus of 500 Å.

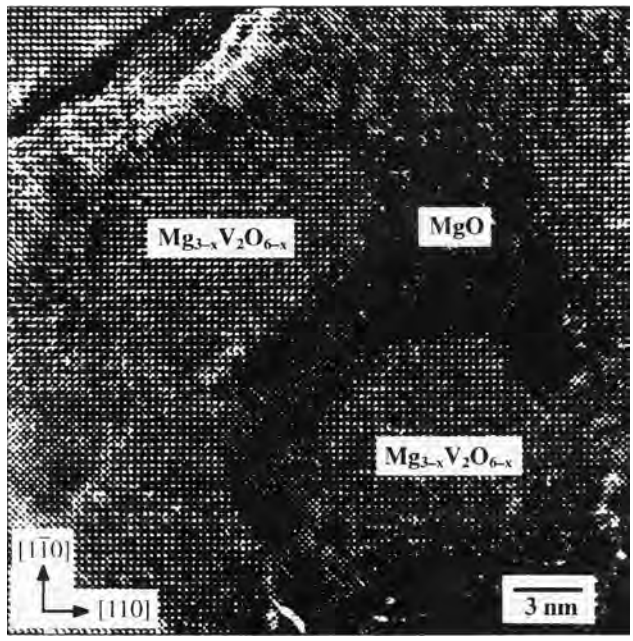

Fig. 6. HRTEM image of $Mg_3V_2O_6$ crystals along [**001**] direction showing the separation of MgO from $Mg_3V_2O_6$.

In contrast to the one weight loss step observed in the reduction of $Mg_3V_2O_8$, oxidation of $Mg_3V_2O_6$ shows two stages of weight gain, one near 300°C and one near 500°C, in the TGA curve. This indicates that a solid solution $Mg_3V_2O_{6+x}$ ($x>0$) possibly exists at temperatures significantly lower than the reduction temperatures. Oxidation of $Mg_3V_2O_6$ powder at 380°C for 60 h in static air results in a deep green powder (~$Mg_3V_2O_{6.31}$ by TGA) and is further oxidized at approximately 500°C to $Mg_3V_2O_8$. Oxidation of crystalline $Mg_3V_2O_6$ is very sluggish. Optical microscopy of the crystals after treatment in air at 800°C for 5 h reveals striations of alternating white and black color.

The reciprocal susceptibilities versus temperature for $Mg_3V_2O_6$ powder and crystals are presented in Fig. 8 and the results are very similar. Above 90 K, a straight line was observed. Below 90 K there is an increase in the susceptibility to about 35 K. This increase was not observed in MgV_2O_4 [21].

4. Conclusions

In conclusion, reduction of magnesium orthovanadate in hydrogen across the temperature range of 560–800°C transforms orthorhombic $Mg_3V_2O_8$ to cubic $Mg_3V_2O_6$. Our studies have shown that the orthovanadate is trans-

Table 3
Cell parameters of $Mg_3V_2O_8$ and $Mg_3V_2O_6$-type phases for the samples obtained under different conditions

Composition	No. of phase	$Mg_3V_2O_8$				$Mg_3V_2O_6$ phase
		a (Å)	*b* (Å)	*c* (Å)	*V* (Å^3)	*a* (Å)
$Mg_3V_2O_8$	1	6.0612(5)	11.4415(6)	8.3185(7)	576.89(6)	
$Mg_3V_2O_8$ [a]	1	6.0597(4)	11.4359(5)	8.3121(4)	576.01(4)	
$Mg_3V_2O_{7.47}$ [b]	2	6.0553(4)	11.4315(9)	8.3085(8)	575.13(6)	8.408(1)
$Mg_3V_2O_{6.57}$ [c]	2	6.0579(8)	11.453(2)	8.3190(8)	577.1(1)	8.4133(8)
$Mg_3V_2O_{6.31}$ [d]	1					8.4164(3)
$Mg_3V_2O_6$ [e]	1					8.4257(2)

[a]$Mg_3V_2O_8$ was treated in H_2 at 620°C for 5 min, [b]in H_2 at 620°C for 1 h, [c]in H_2 at 620°C for 2 h. [d]$Mg_3V_2O_6$ was treated in air at 380°C for 60 h. [e]$Mg_3V_2O_8$ was treated in H_2 at 920°C for 12 h.

formed in a topochemical reaction with the excess magnesium cations distributed on octahedral sites in the ''stuffed'' spinel structure.

Acknowledgements

The authors like to thank Charlotte L. Stern, Keven R. Heier, Dr. Timothy McCarthy for assistance with measurements, Prof. Wolfgang Sachtler and Dr. Kenji Ochi for discussions, and wish to thank Dr. Larry Cirjak and acknowledge a Research Award from BP America, Inc., the National Science Foundation (NSF) (No. DMR-9412971) and the MRC of Northwestern University Supported by NSF (No. DMR-9120521) for support.

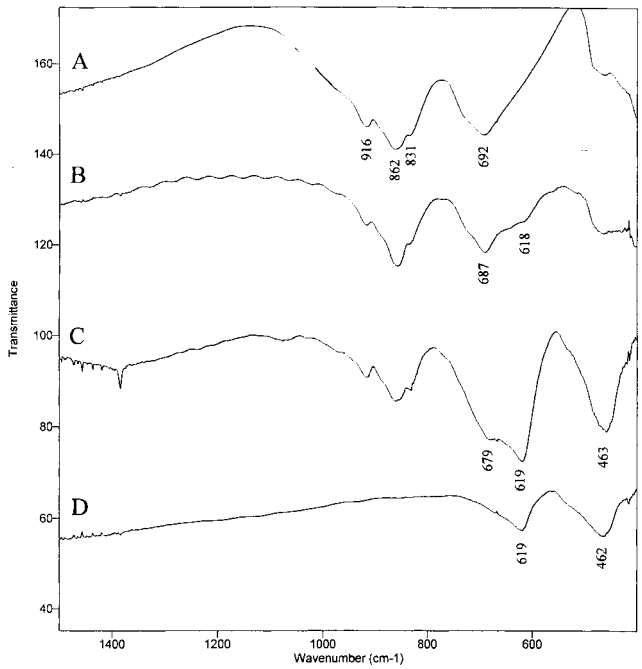

Fig. 7. IR spectra of $Mg_3V_2O_8$ (A), $Mg_3V_2O_{7.47}$ (B), $Mg_3V_2O_{6.57}$ (C) and $Mg_3V_2O_6$ (D). (B) and (C) are composed of $Mg_3V_2O_8$ phase and $Mg_3V_2O_6$-type phase. The cell parameters for each phase are given in Table 3.

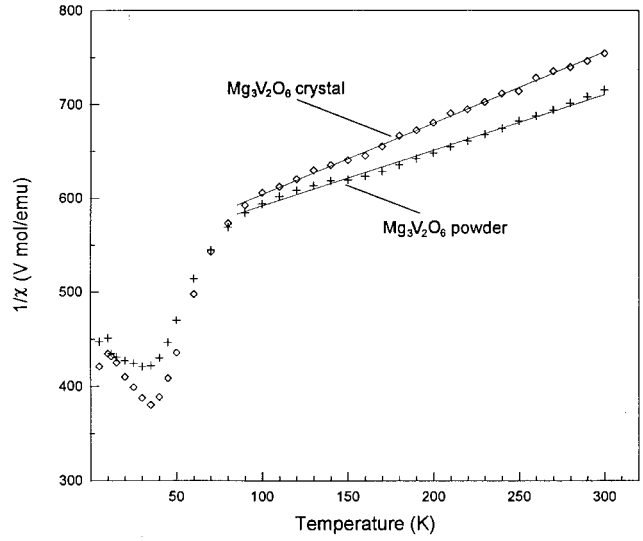

Fig. 8. Reciprocal magnetic susceptibilities versus temperature for $Mg_3V_2O_6$ powder and crystals.

References

[1] M.A. Chaar, D. Patel, M.C. Kung, H.H. Hung, J. Catal. 105 (1987) 483.
[2] O.S. Owens, H.H. Kung, J. Mol. Catal. 79 (1993) 265.
[3] W.D. Harding, H.H. Kung, V.L. Kozhevnikov, K.R. Poeppelmeier, J. Catal. 144 (1993) 597.
[4] S.R.G. Carrazan, C. Peres, J.P. Bernard, J. Catal. 158 (1996) 452.
[5] L.E. Cadus, M.C. Abello, M.F. Gomez, Ind. Eng. Chem. Res. 35 (1996) 14.
[6] V. Soenen, J.M. Herrmann, J.C. Volta, J. Catal. 159 (1996) 410.
[7] N. Krishnamachari, C. Calvo, Canad. J. Chem. 49 (1971) 1629.
[8] G.W. Coulston, S.R. Bare, H.H. Kung, K. Birkeland, G.K. Bethke, R. Harlow, N. Herron, P.L. Lee, Science 275 (1997) 191.
[9] X.D. Wang, C.L. Stern, K.R. Poeppelmeier, J. Alloys Comp. 243 (1996) 51.
[10] N. Walker, D. Stuart, Acta Crystallogr. 39A (1983) 158.

[11] R. Wollast, A. Tazairt, in: E.M. Levin, H.F. McMurdie (Eds.), Phase Diagrams for Ceramists, 1975 Supplement, American Ceramic Society, 1975, p. 118.
[12] M.S. Najjar, in: R.S. Roth (Ed.), Phase Diagrams for Ceramists, Vol. XI, American Ceramic Society, 1995, p. 91.
[13] W.I.F. David, M.M. Thackeray, L.A. de Picciotto, J.B. Goodenough, J. Solid State Chem. 67 (1987) 316.
[14] G.A. Lager, T. Armbruster, F.K. Ross, F.J. Rotella, J.D. Jorgensen, J. Appl. Cryst. 14 (1981) 261.
[15] R.J. Cava, D.W. Murphy, S. Zahurak, A. Santoro, R.S. Roth, J. Solid State Chem. 53 (1984) 64.
[16] L.A. de Picciotto, M.M. Thackeray, Mat. Res. Bull. 20 (1985) 1409.
[17] J. Rodriguez-Carvajal, Collected Abstracts of Powder Diffraction Meeting, Toulous, France, 1990, p. 127.
[18] P.L. Gai, K. Kourtakis, Science 267 (1995) 661.
[19] Y. Tamaura, M. Tabata, Nature 346 (1990) 255.
[20] R. Iordanova, Y. Dimitriev, V. Dimitrov, D. Klissurski, J. Non-Cryst. Solids 167 (1994) 74.
[21] G. Blasse, J.F. Fast, Philips Res. Repts. 18 (1963) 393.